Developmental Cell
Short Article

Membrane Shape Modulates Transmembrane Protein Distribution

Sophie Aimon,[1,2,3,4] Andrew Callan-Jones,[5] Alice Berthaud,[1,2,3,6] Mathieu Pinot,[1,6,7] Gilman E.S. Toombes,[8,9,*] and Patricia Bassereau[1,2,3,6,9]
[1]Centre de Recherche, Institut Curie, Paris F-75248, France
[2]CNRS, PhysicoChimie Curie, UMR168, Paris F-75248, France
[3]Université Pierre et Marie Curie, Paris F-75252, France
[4]Kavli Institute for Brain and Mind, UCSD, La Jolla, CA 92093, USA
[5]Laboratoire Matière et Systèmes Complexes, CNRS/Université Paris-Diderot, UMR 7057, 75205 Paris Cedex 13, France
[6]CelTisPhyBio Labex, Paris Sciences et Lettres, 75005 Paris, France
[7]CNRS, Subcellular Structure and Cellular Dynamics, UMR144, Paris F-75248, France
[8]Molecular Physiology and Biophysics Section, Porter Neuroscience Research Center, National Institute of Neurological Disorders and Stroke, National Institutes of Health, Bethesda, MD 20892-3017, USA
[9]These authors contributed equally to this work
*Correspondence: gilman.toombes@nih.gov
http://dx.doi.org/10.1016/j.devcel.2013.12.012

SUMMARY

Although membrane shape varies greatly throughout the cell, the contribution of membrane curvature to transmembrane protein targeting is unknown because of the numerous sorting mechanisms that take place concurrently in cells. To isolate the effect of membrane shape, we used cell-sized giant unilamellar vesicles (GUVs) containing either the potassium channel KvAP or the water channel AQP0 to form membrane nanotubes with controlled radii. Whereas the AQP0 concentrations in flat and curved membranes were indistinguishable, KvAP was enriched in the tubes, with greater enrichment in more highly curved membranes. Fluorescence recovery after photobleaching measurements showed that both proteins could freely diffuse through the neck between the tube and GUV, and the effect of each protein on membrane shape and stiffness was characterized using a thermodynamic sorting model. This study establishes the importance of membrane shape for targeting transmembrane proteins and provides a method for determining the effective shape and flexibility of membrane proteins.

INTRODUCTION

The targeting of transmembrane proteins to specific cellular regions is essential for cell function (Cobbold et al., 2003). For example, neuronal information processing requires that specific voltage-gated ion channels with distinct biophysical properties are localized in distinct regions of the neuronal membrane (i.e., soma, dendrites, and axon) (Lai and Jan, 2006). Numerous targeting mechanisms contribute to protein enrichment in trafficking vesicles of the secretory pathway and lateral redistribution after delivery to the acceptor membrane. Much work has focused on specific protein-protein interactions, but manipulating membrane properties has also been shown to alter targeting, suggesting the importance of membrane-based sorting mechanisms (van Meer and Sprong, 2004). Membrane shape is particularly compelling, because some membranes within the cell (e.g., transport vesicles, neurites, and endocytotic pits) are highly curved with radii as small as 20 nm (Nägerl et al., 2008), and many trafficking events involve large changes in membrane curvature (McMahon and Gallop, 2005). However, efforts to study the effect of membrane shape on transmembrane protein distribution in vivo have been impeded by an inability to control membrane curvature without simultaneously affecting other targeting mechanisms (Hägerstrand et al., 2006). Ab initio simulations (e.g., molecular dynamics) are also challenging because the required large system size and long simulation times are currently prohibitive (Callenberg et al., 2012; Chandler et al., 2008). Thus, despite numerous proposals (Markin, 1981; McMahon and Gallop, 2005), it is unknown whether the distributions of typical transmembrane proteins are sensitive to membrane shape.

To address this question, we used an in vitro system to isolate the effects of membrane curvature. As shown in Figure 1A, the relatively flat membrane of a giant unilamellar vesicle (GUV) is connected to a highly curved nanotube. Using the micropipette pressure to control the membrane tension, the radius of the membrane tube, R, can be adjusted from 100 to 7 nm, which reaches the highest membrane curvatures (c = 1/R) observed in cells (McMahon and Gallop, 2005; Nägerl et al., 2008). Similar in vitro approaches have previously been used to study the effects of curvature on lipids and proteins whose function is to sense or control membrane shape (e.g., BAR proteins, dynamin, and reticulons) (Heinrich et al., 2010; Hsieh et al., 2012; Hu et al., 2008; Parthasarathy et al., 2006; Sorre et al., 2009, 2012; Tian and Baumgart, 2009).

As model proteins we chose two well-studied tetrameric channels of similar molecular mass: AQP0, a member of the major intrinsic protein family (Gonen et al., 2005), and KvAP, a bacterial member of the voltage-gated ion channel family (Jiang et al., 2003). Both have previously been reconstituted into GUVs, and

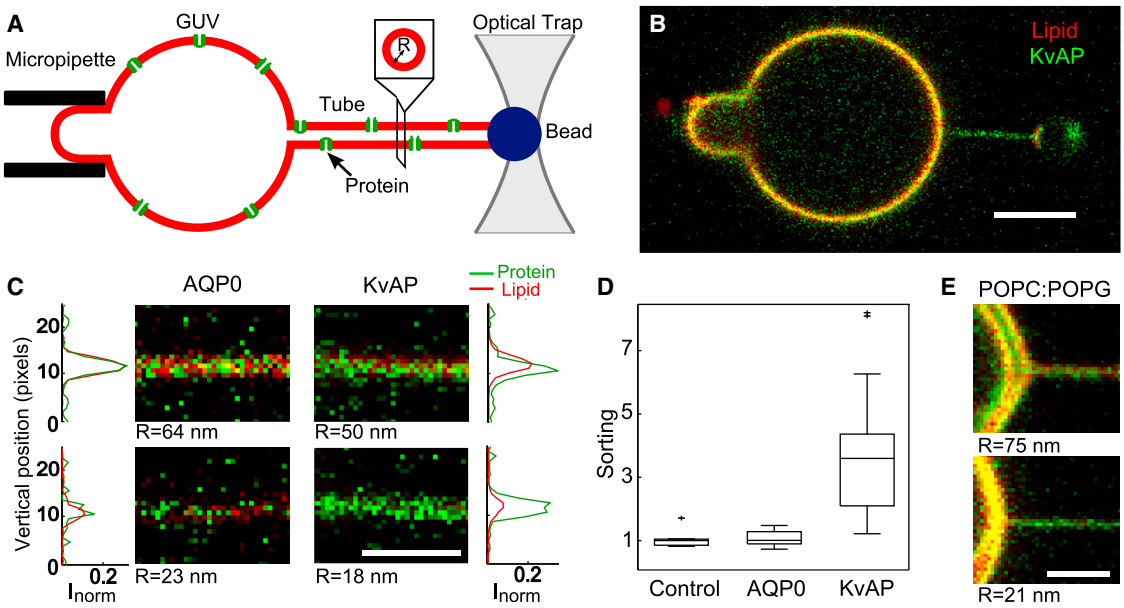

Figure 1. KvAP Is Enriched in Curved Membranes, whereas AQP0 Is Not

(A) Schematic of tube assay. A bead in an optical trap is used to pull a membrane tube from a GUV held by a micropipette. The pressure in the micropipette controls the membrane tension and resultant tube radius, R, whereas the concentrations of lipid and protein in the tube are measured by confocal fluorescence microscopy (see also Figure S1 and Table S1).

(B) Confocal image of a tube (radius R = 14 nm) pulled from a GUV containing reconstituted KvAP (GUV protein density, $\rho_{GUV} = 70\ \mu m^{-2}$). The membrane (red) was marked with a fluorescent lipid (Texas Red DHPE), whereas the protein (green) was labeled with Alexa 488. Contrast has been enhanced, and green and red intensities have been scaled to match in the GUV (which is thus yellow). The green color of the tube therefore reflects protein enrichment in the tube (relative to the GUV). Scale bar, 5 μm.

(C) Images and intensity profiles of tubes pulled from GUVs containing AQP0 (left, $\rho_{GUV} \sim 100\ \mu m^{-2}$) or KvAP (right, $\rho_{GUV} = 70\ \mu m^{-2}$) for large (R ~60 nm) and small (R ~20 nm) tube radii. Green and red intensities have been scaled to match in the GUV and corrected for the effects of the light polarization (PCF). The low protein density causes large fluctuations in the green channel, which are smaller in the intensity profile due to the averaging along the tube. Scale bar, 2 μm.

(D) Box plots comparing the sorting ratio for tubes (R = 25 ± 10 nm) pulled from GUVs containing a green fluorescent lipid (control), AQP0, or KvAP. The median is represented with a line; the box represents the 25th to 75th percentiles; and error bars show the 5th–95th percentile. The average sorting ratios for the lipid control (mean = 1.1, SD = 0.3, n = 7 GUVs) and AQP0 (mean = 1.1, SD = 0.2, n = 12) are similar, whereas KvAP is noticeably enriched in the tubes (mean = 3.5, SD = 1.7, n = 41).

(E) Effect of the GUV composition on KvAP sorting. Confocal images of large (R = 75 nm) and small (R = 21 nm) membrane tubes extracted from GUVs formed from a different lipid mixture, POPC/POPG (9:1 by mass). Defects were more common with this lipid composition, and a second, smaller vesicle is nested inside the main "GUV." Scale bar, 3 μm.

as channels their function is not directly related to membrane shape. However, it has been proposed that membrane curvature may modulate the distribution of Kv channels (McMahon and Gallop, 2005), because some Kv channel types localize in very curved regions of neuronal membranes (dendrites or axons) (Lai and Jan, 2006), and the Kv voltage-sensing domain is believed to distort the surrounding membrane (Bond and Sansom, 2007). In contrast, AQP0 is found in flat lens membranes in vivo (Zampighi et al., 2002) and, when reconstituted in vitro, can form flat, single-layered two-dimensional (2D) crystals (Gonen et al., 2005).

RESULTS

Measuring Curvature-Induced Protein Sorting In Vitro

Membrane nanotubes were pulled from GUVs containing fluorescently labeled protein (KvAP or AQP0-labeled with Alexa 488) and a fluorescent lipid (Texas Red DHPE or BODIPY-TR Ceramide). Because the distribution of fluorescent lipids is approximately uniform in our system (Sorre et al., 2009), the enrichment of the proteins in the tube can be measured by comparing their fluorescence to the fluorescence of lipids. In Figure 1B, the lipid (red) and protein (green) fluorescence intensities have been scaled to match at the GUV equator. If the protein and lipid had equal affinities for the membrane tube, the fluorescence intensities would be equal and the tube would appear yellow. Instead, the tube is clearly green, indicating that the protein-to-lipid ratio in the curved membrane tube is greater than that in the flatter GUV membrane. This relative protein enrichment can be quantified by the sorting ratio, S, defined as

$$S = \frac{PCF_{protein}}{PCF_{lipid}} \times \frac{I_{tube}^{protein} / I_{tube}^{lipid}}{I_{GUV}^{protein} / I_{GUV}^{lipid}}, \qquad \text{(Equation 1)}$$

where the polarization correction factors (PCFs) account for fluorophore orientation (as described in the Supplemental Experimental Procedures and Table S1 available online) and $I_{tube/GUV}^{protein/lipid}$ is the protein (or lipid) fluorescence intensity of the tube (or GUV) (Sorre et al., 2009).

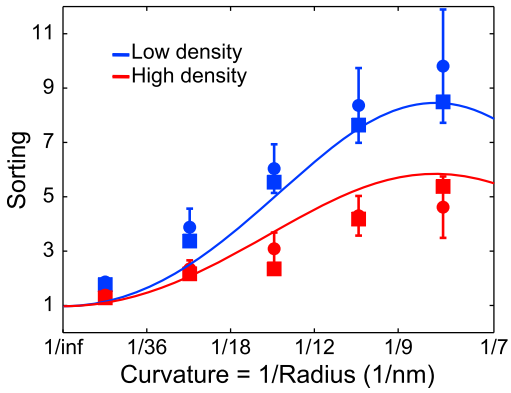

Figure 2. KvAP Enrichment as a Function of Tube Curvature

Sorting as a function of curvature, c = 1/R, for GUVs with high (red; mean = 1,705 μm^{-2}, SD = 414 μm^{-2}) and low (blue; mean = 162 μm^{-2}, SD = 70 μm^{-2}) protein densities. Points are the mean of binned sorting values, error bars are ± SEM, and squares are the median (numerical values in Table S2). Solid lines are fits of the sorting model (see Equation S26 in Supplemental Experimental Procedures; Figure S2) to the median, and taking A_{prot} = 45 nm^2, we obtain κ_p = 38.5 k_BT and c_p = (1/25) nm^{-1}.

KvAP Is Strongly Enriched in Curved Membranes, whereas AQP0 Is Not

Figure 1C shows images of membrane tubes formed from GUVs containing AQP0 and KvAP, along with the resulting intensity profiles normalized by the intensity at the GUV equator and corrected by the PCF. For the larger tube formed from an AQP0-containing GUV (R = 64 nm), the protein (green) and lipid (red) fluorescence signals are similar (sorting ratio, S = 0.93 ± 0.10), and thus the composition of the membrane tube is indistinguishable from that of the GUV. When the tube radius was then reduced to R = 23 nm, the protein fluorescence (green) decreased and the absolute signal was so low that fluctuations in the number of fluorophores per voxel are clearly evident. Nevertheless, when the protein fluorescence is averaged along the entire length of the tube, the normalized intensity is again similar to the lipid normalized intensity with a sorting ratio of S = 1.1 ± 0.4. Thus, it appears that membrane curvature has little effect on AQP0 concentration. This measurement was performed for multiple GUVs and the sorting ratio measured for membrane tubes with radii between 15 nm and 35 nm. To gauge experimental precision, control experiments were also performed using GUVs containing the green fluorescent lipid, BODIPY-FL HPC, which was previously shown to be uniformly distributed in the absence of the proximity of a demixing point or interaction with proteins (Sorre et al., 2009). As shown in Figure 1D, the sorting ratio for AQP0 (mean = 1.1, SD = 0.2, n = 12) was quite similar to that for the control experiment (mean = 1.1, SD = 0.3, n = 7). Thus, the distribution of AQP0 does not appear to be significantly influenced by membrane curvature.

In contrast, the distribution of KvAP appears to be sensitive to membrane curvature. As shown in Figure 1C (right panels), the protein was already enriched even in a large tube (R = 50 nm, S = 1.6 ± 0.1), and this protein enrichment increased with membrane tube curvature, reaching S = 4.0 ± 0.8 for R = 18 nm. Repeating this experiment with multiple GUVs gave an average sorting ratio of S = 3.5 (SD = 1.7, n = 41 GUVs) for tube radii between 15 and 35 nm (Figure 1D), and KvAP enrichment was also observed in membrane tubes extracted from GUVs formed using different preparation protocols (Figure S1B). As discussed below, the variability in protein enrichment in individual membrane tubes may in part be due to the effect of protein density on sorting. Thus, unlike AQP0, KvAP was measurably enriched in curved membranes.

The sorting of lipids and peripheral membrane proteins can be greatly altered when membrane components have nonideal interactions (Sorre et al., 2009). In an effort to exclude such effects, the Egg-PC/Egg-PA (9:1 by mass) composition was selected because it showed no signs of phase separation or curvature-induced lipid sorting (using fluorescent lipid probes) and has comparable bulk properties (bending modulus, surface charge, curvature stress) to membranes extracted from cells. However, whereas 10%–20% of eukaryotic plasma membrane lipids typically have a negatively charged head group, phosphatidic acid (PA) is usually a minor component (e.g., <2%) (van Meer et al., 2008). To confirm that the curvature-induced sorting was not due to any specific effects of PA, KvAP was reconstituted in the fully synthetic lipid mixture POPC/POPG (9:1 by mass). Like PA, PG is negatively charged at physiological pH, and biophysical studies show that it mixes well with PC lipids (Blosser et al., 2013). As shown in Figure 1E, GUVs formed from POPC/POPG lipids exhibited a significant, curvature-dependent enrichment of KvAP (average sorting ratio = 3.7; SD = 2.3; n = 11; median radius = 32 nm), suggesting that the enrichment of KvAP is not due to interactions with specific lipids but is rather due to the direct coupling of membrane shape to protein distribution.

Protein density was previously shown to affect the curvature-induced sorting of peripheral membrane proteins (Sorre et al., 2012). To determine how protein density influenced KvAP sorting, GUVs with a lower protein density were prepared by diluting the small proteoliposomes with pure lipid liposomes. Figure 2 shows the enrichment of KvAP as a function of curvature for GUV populations in two density ranges: approximately 150 proteins/μm^2 (corresponding to an area fraction of ~1%) and approximately 1,500 proteins/μm^2 (respectively, ~10%). Curvature-dependent sorting is evident at both low and high density. At high density, the total amount of protein that redistributed (i.e., $\rho_{tube} - \rho_{GUV}$) was greater, but the relative enrichment (i.e., ρ_{tube}/ρ_{GUV}) was reduced. This result suggests the existence of a mechanism that limits the total amount of protein that can redistribute, as will be discussed in more detail below (see also Figure S2).

Transmembrane Proteins Can Exchange between the GUV and Tube

The shape of the neck joining the GUV to the tube resembles the membrane at the base of neurites or cilia, where diffusion impairment has been observed (Ashby et al., 2006; Caudron and Barral, 2009). Although proteins, such as septins, play a crucial role in cellular diffusion barriers, membrane geometry could also contribute (Domanov et al., 2011). It is therefore important to determine whether the neck impedes diffusion between the GUV and the membrane tube, thereby preventing the protein distribution from equilibrating in our experiments.

Several lines of evidence indicate that AQP0 and KvAP were able to freely diffuse across the neck connecting the GUV to

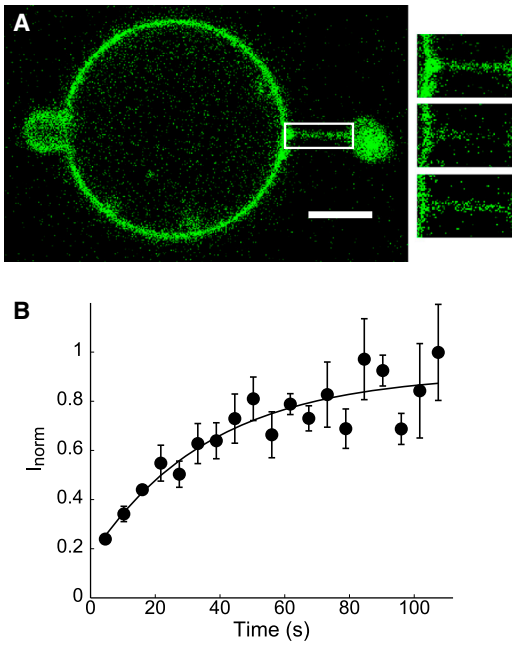

Figure 3. KvAP Can Freely Diffuse in and out of the Tube

(A) KvAP fluorescence recovery in the tube (R = 20 nm, L = 6 μm) after photobleaching the zone indicated by the white square. Right: images of the tube before (top), 5 s after (middle), and 110 s after (bottom) photobleaching. Scale bar, 6 μm.

(B) Intensity of KvAP fluorescence in the tube (relative to the GUV body and to value before bleaching) as a function of time. Data were averaged over five time points to reduce noise, and error bars are ± SEM. The solid line represents a fit using $I_{norm}(t) = I_{\infty} \times (1 - F \times \exp(-t/\tau))$ and τ = 38 s. See Figure S3 for additional data.

the membrane tube. First, after pulling a tube from a GUV with a low density of KvAP, the fluorescence intensity in the tube gradually increased to a higher level, consistent with protein diffusing into the tube (Figure S3A). Next, fluorescence recovery after photobleaching (FRAP) experiments were used to systematically determine if the membrane neck presented a measurable barrier to protein diffusion. As shown in Figure 3A, a tube was formed from a GUV containing fluorescently labeled KvAP, and after waiting 2 min for the tube composition to equilibrate, the fluorophores in the tube were bleached by imaging at full laser power. Fluorescence recovery in the tube was then monitored by imaging at low laser power. The right panel of Figure 3A shows the protein fluorescence in the tube before, 5 s after photobleaching, and 110 s after photobleaching. The diffusion of proteins from the GUV back into the membrane tube is clear, and fitting the recovery curve (Figure 3B) with an exponential gives a relaxation time of 38 s for this example. This time is shorter than the waiting time (approximately 2 min) between tension increment and measurement in the sorting experiments, suggesting that KvAP and AQP0 densities in these experiments were at equilibrium.

Repeated FRAP experiments on GUVs containing AQP0 (Figure S3B) or KvAP confirmed that both proteins can cross the tube neck. Although some bleaching occurred during recovery, fitting the fluorescence recovery curves with a model of free diffusion in the tube (Berk et al., 1992) yielded D_{tube} = 0.5 ± 0.3 $\mu m^2/s$ (mean ± SD, n = 9, R = 25 ± 10 nm) for KvAP and D_{tube} = 1.1 ± 0.4 $\mu m^2/s$ (mean ± SD, n = 4, R = 50 ± 14 nm) for AQP0 (see the Supplemental Experimental Procedures for more details). For KvAP, both the diffusion coefficient and its reduction with decreasing tube radius are in quantitative agreement with previous measurements of KvAP diffusion in tubes using single-particle tracking (Domanov et al., 2011) (Figure S3C). Thus, the recovery matches free protein diffusion through the neck and along the tube, and there is no detectable diffusion barrier at the neck. Furthermore, the diffusion coefficients for KvAP and AQP0 are consistent with the diffusion of single transmembrane proteins in a confined geometry (Daniels and Turner, 2007), arguing against the presence of large clusters in the membrane (Domanov et al., 2011; Ramadurai et al., 2009). These observations establish that proteins can traverse the neck of the tube, even for tube radii as small as 15 nm, and imply that the enrichment described in the previous section paragraph is an equilibrium phenomenon.

Protein Shape and Stiffness Can Account for Curvature-Driven Sorting

Forming curved structures, such as transport vesicles, dendrites, or the nanotubes used in these experiments, requires energy to bend the membrane (Markin, 1981). This membrane bending energy is then affected by transmembrane proteins that change the unstressed shape or the stiffness of the membrane. For example, the membrane bending energy of the nanotube can be reduced by enriching proteins that soften the membrane or bend the membrane outward, and/or by depleting proteins that stiffen the membrane or bend it inward (Figure S2B). At equilibrium, this reduction in membrane bending energy is counterbalanced by the entropic cost of distributing proteins nonuniformly. Thus, by modeling the membrane bending energy and mixing entropy, it should be possible to relate the curvature-driven sorting of AQP0 and KvAP to their effects on membrane shape and stiffness.

Because of the complexity of protein-membrane interactions and the large scale of the system, theoretical treatments have typically used a continuum approach in which the membrane is modeled as a thin (quasi-2D), fluid film in which proteins freely diffuse (Leibler, 1986; Markin, 1981; Netz and Pincus, 1995). The model presented here is based on the work of Markin (1981). The protein mixing entropy is approximated by the Van der Waals equation of state (Singh et al., 2012), whereas the membrane bending energy is calculated using the elastic response of a thin, cylindrical sheet,

$$U_{bending} = A \times \frac{\kappa}{2} \times (c - c_0)^2, \qquad \text{(Equation 2)}$$

where A is the membrane area, κ is the membrane bending modulus, c is the curvature, and c_0, the membrane spontaneous curvature, describes the resting, unstressed shape of the membrane.

Proteins then alter this bending energy by changing the shape (c_0) and stiffness (κ) of the membrane (Markin, 1981; Netz and Pincus, 1995). The effect of a protein on membrane shape is described by the protein spontaneous curvature, c_p, which corresponds to the curvature of an unstressed membrane containing a saturating density of the protein and reflects the orientation of the membrane at the protein-lipid interface (Figure S2A).

Similarly, the effect of a protein on membrane stiffness can be described by the effective protein bending modulus, κ_p, which incorporates both the intrinsic stiffness of the protein and its effects on the surrounding membrane. As described in the Supplemental Experimental Procedures, the protein distribution can then be calculated by determining the membrane tube composition that minimizes the total free energy of the curved membrane tube coupled to an essentially flat GUV.

In general, the resulting equations require a numerical, self-consistent solution because the transfer of each molecule between flat and curved membranes alters the membrane bending energy remaining to drive further transfers (Sorre et al., 2012). However, the key features of the model can be understood by considering several special cases. First, when the total protein concentration is very low, the redistribution of proteins has a negligible effect on the membrane bending energy. Sorting is then only limited by the entropic penalty and the degree of enrichment has a simple dependence on the protein size, shape, and stiffness (Equation S28 in Supplemental Experimental Procedures; Figure S2C). In contrast, at higher protein concentrations, even a modest (e.g., 2-fold) enrichment/depletion can lower the membrane bending energy enough to limit further protein redistribution, and the protein distribution must be solved self-consistently. This reduction of protein sorting at higher protein densities is evident both in a parametric solution of a membrane containing a single protein species (Figure S2E) and an approximate, power-series solution for the experimental system (Figure S2F). Thus, the model predicts that transmembrane proteins that cause larger changes to membrane shape or stiffness will be more strongly enriched or depleted (Derganc, 2007), whereas the relative enrichment/depletion (e.g., sorting ratio) will decrease at higher protein concentrations.

In order to model the experiments, GUVs were assumed to contain equal amounts of each protein insertion (i.e., cytosolic domain facing into/out from the GUV). In general, the effects of curvature on the two insertions do not cancel and so the total protein concentration of the tube varies with curvature, as shown in Figure S2D.

For AQP0, the lack of observable, curvature-driven sorting (Figure 1D) places strong restrictions on how it influences the membrane shape and stiffness (see the Supplemental Experimental Procedures). First, the preferred shape of the membrane surrounding AQP0 must be fairly flat ($|c_p| < 1/50\ \mathrm{nm}^{-1}$). This result agrees well with the relatively uniform, cylindrical profile of the AQP0-lipid interface, the ability of AQP0 to form flat crystalline arrays in the membrane junctions between lens fiber cells, and the observation that among membrane proteins that can be reconstituted to form single-layered crystals, AQP0 is unusual because all the molecules are inserted in the same direction (Gonen et al., 2005). The absence of strong curvature-driven sorting also requires that AQP0 does not significantly change the membrane stiffness ($0.7 < \kappa_p/\kappa_{lipid} < 1.3$). This may seem surprising because proteins are generally assumed to be stiffer than lipid bilayers (Markin, 1981), but it is important to recall that κ_p describes the total effect of AQP0 on the membrane stiffness and proteins may disrupt the packing and thus soften the annular lipids surrounding them (Fosnaric et al., 2006).

To perform a quantitative comparison of the model to the experimental sorting measurements of KvAP, Equation S26 (see Supplemental Experimental Procedures) was minimized numerically, and the protein shape, c_p, and protein rigidity, κ_p, were adjusted to simultaneously fit both the high and low protein density data shown in Figure 2. The theoretical model accounts well for the reduced sorting at the higher protein concentration, and the best fit was obtained if KvAP caused a modest increase in membrane rigidity ($\kappa_p \approx 1.5 \times \kappa_{lipid}$) but was nevertheless enriched because it bends the membrane ($|c_p| \approx 1/25\ \mathrm{nm}^{-1}$). The fitted protein spontaneous curvature, $|c_p| \approx 1/25\ \mathrm{nm}^{-1}$, corresponds to an average tilt at the protein-membrane interface ($R_p \sim 4$ nm) of $\sim 10°$. Because the GUVs contained both protein insertions, these experiments cannot be used to determine whether KvAP bends the membrane toward or away from the cell interior in vivo (see the Supplemental Experimental Procedures and Figures S1C–S1E for discussion of orientation effects). However, the magnitude of the deformation is consistent with theoretical estimates based on the effects of membrane state on Kv channel function (Reeves et al., 2008).

This simple model can simultaneously account for both the measured curvature and density dependence of KvAP sorting purely in terms of its effect on membrane shape and stiffness. However, additional effects may be important for curvature-driven sorting, especially in biological systems. While these experiments were performed with lipids that mix well, the plasma membrane has been shown to readily separate into inhomogeneous domains (Veatch et al., 2008), and such nonideal mixing could greatly enhance curvature-driven sorting. Additionally, the model assumes that proteins have a single, well-defined conformation, but some membrane proteins undergo significant conformational changes that would clearly modify their curvature-dependent distributions (Reeves et al., 2008). Finally, the elastic model of the membrane bending energy is only a rough approximation for highly curved membranes (e.g., synaptic vesicles). The effects of nonideal mixing, multiple protein conformations, and nonlinear elasticity could be incorporated in a more complicated treatment, but the present model describes the central features of curvature-induced transmembrane protein sorting and is consistent with the experimental data.

DISCUSSION

Despite numerous proposals that membrane shape might directly modulate the distribution of transmembrane proteins (Bozic et al., 2006; Markin, 1981), the role of membrane curvature in transmembrane protein targeting has remained largely unexplored (McMahon and Gallop, 2005) because of the difficulties in controlling membrane shape and the presence of multiple targeting mechanisms in cells (Hägerstrand et al., 2006). Using an in vitro approach, we have directly demonstrated that membrane shape alone can modulate the distribution of polytopic, transmembrane proteins. Furthermore, this curvature-driven sorting should be an equilibrium effect because FRAP measurements showed that both proteins could freely exchange between curved and flat membranes. Indeed, a simple thermodynamic model of protein sorting based on the effect of the proteins on membrane shape and stiffness (Markin, 1981) could account for both the curvature and density dependence of sorting.

Proteins that control membrane shape are thought to use specific mechanisms to sense and generate membrane

deformations, such as the insertion of amphipathic helices (e.g., epsin) or hairpins (e.g., reticulons), and oligomerization into a curved scaffold (e.g., dynamin) (McMahon and Gallop, 2005). Such mechanisms may be important for proteins that deform the membrane, but the distribution of a protein can be quite sensitive to membrane shape without significantly altering the energy needed to curve the membrane (Figure S2G). Indeed, the thermodynamic model predicts that curvature-induced sorting should occur unless a protein has both a minimal effect on membrane stiffness and a very uniform transmembrane profile (like AQP0). Thus, membrane curvature is likely to modulate the distributions of many transmembrane proteins and should also influence protein function (e.g., ion channel gating or receptor activation) because changes to protein conformation will alter the protein effective shape.

At present, one cannot readily predict the curvature sensitivity of a specific transmembrane protein. However, even when the detailed structure of a transmembrane protein is unknown, our in vitro system provides a way to quantify the sensitivity of specific proteins to membrane curvature and characterize the protein's effective shape and flexibility in the lipid bilayer. This information will be crucial for understanding how proteins interact with the surrounding membrane and also provide a strong test for future ab initio calculations.

In conclusion, this work demonstrates that the contribution of membrane shape to targeting proteins during trafficking and localization at the membrane needs to be taken into account and motivates future efforts to measure the effects of membrane curvature on transmembrane protein activity.

EXPERIMENTAL PROCEDURES

Protein Reconstitution

KvAP and AQP0 were purified (Aimon et al., 2011; Berthaud et al., 2012), labeled with Alexa 488 (green), and reconstituted in Egg-PC/Egg-PA (9:1 by mass) GUVs as described previously (Aimon et al., 2011). The red fluorescent lipids Texas Red DHPE or BODIPY-TR ceramide were included at 0.25% by mole to allow membrane visualization, and the protein density of individual GUVs (ρ_{GUV}) was measured using the green fluorescence intensity as described in Aimon et al. (2011) (see the Supplemental Experimental Procedures for further details).

Membrane Tube Extraction

Using the microscopy setup described in Sorre et al. (2012), a micropipette was used to hold a GUV. A membrane tube was then extracted from the GUV using a polystyrene bead trapped in an optical tweezer. The aspiration pressure in the micropipette was used to control the tube radius, R, which was measured by comparing the lipid fluorescence intensity of the membrane tube to that of the GUV equator (see Figure S1 and Supplemental Experimental Procedures for further details). After each change in tube radius, the protein and lipid distributions were imaged with a confocal microscope after waiting approximately 2 min for the tube composition to equilibrate.

FRAP Experiments

FRAP measurements were performed using a Nikon AR-1 or a Nikon C1 confocal microscopes. A tube was formed from a GUV containing fluorescently labeled KvAP or AQP0 as described above. After measuring the initial protein fluorescence, the fluorophores in the tube were bleached by imaging at full laser power. The fluorescence recovery of the tube was then monitored by imaging at low (approximately 5%) laser power, in an effort to limit photobleaching during the recovery phase (see Figure S3 and the Supplemental Experimental Procedures for more details).

SUPPLEMENTAL INFORMATION

Supplemental Information includes Supplemental Experimental Procedures, three figures, and two tables and can be found with this article online at http://dx.doi.org/10.1016/j.devcel.2013.12.012.

ACKNOWLEDGMENTS

The authors thank J.B. Manneville for access to his FRAP setup, F. Quemeneur and C. Prevost for help with the optical trap, F. Faqir, J. Manzi, M. Garten, and S. Mangenot for help with biochemistry, T. Bornschloegl for discussions, and B. Goud, L. Johannes, R. Martin, J. Kalia, A. Manzo, and T. Katsuki for comments on the manuscript. The authors acknowledge financial support from the Agence Nationale de la Recherche (grant BLAN-0057-01), the Fédération "Dynamique des systèmes complexes hors équilibre" of the University Pierre et Marie Curie, the Institut Curie, and the "Fondation pour la Recherche Médicale" (to S.A.), CNRS action "Prise de Risque" (to A.B.), a Marie Curie fellowship (to G.E.S.T.), and the French research consortium "CellTiss" (to P.B.).

Received: March 20, 2013
Revised: July 22, 2013
Accepted: December 19, 2013
Published: January 27, 2014

REFERENCES

Aimon, S., Manzi, J., Schmidt, D., Poveda Larrosa, J.A., Bassereau, P., and Toombes, G.E. (2011). Functional reconstitution of a voltage-gated potassium channel in giant unilamellar vesicles. PLoS ONE *6*, e25529.

Ashby, M.C., Maier, S.R., Nishimune, A., and Henley, J.M. (2006). Lateral diffusion drives constitutive exchange of AMPA receptors at dendritic spines and is regulated by spine morphology. J. Neurosci. *26*, 7046–7055.

Berk, D.A., Clark, A., Jr., and Hochmuth, R.M. (1992). Analysis of lateral diffusion from a spherical cell surface to a tubular projection. Biophys. J. *61*, 1–8.

Berthaud, A., Manzi, J., Pérez, J., and Mangenot, S. (2012). Modeling detergent organization around aquaporin-0 using small-angle X-ray scattering. J. Am. Chem. Soc. *134*, 10080–10088.

Blosser, M.C., Starr, J.B., Turtle, C.W., Ashcraft, J., and Keller, S.L. (2013). Minimal effect of lipid charge on membrane miscibility phase behavior in three ternary systems. Biophys. J. *104*, 2629–2638.

Bond, P.J., and Sansom, M.S. (2007). Bilayer deformation by the Kv channel voltage sensor domain revealed by self-assembly simulations. Proc. Natl. Acad. Sci. USA *104*, 2631–2636.

Bozic, B., Kralj-Iglic, V., and Svetina, S. (2006). Coupling between vesicle shape and lateral distribution of mobile membrane inclusions. Phys. Rev. E Stat. Nonlin. Soft Matter Phys. *73*, 041915.

Callenberg, K.M., Latorraca, N.R., and Grabe, M. (2012). Membrane bending is critical for the stability of voltage sensor segments in the membrane. J. Gen. Physiol. *140*, 55–68.

Caudron, F., and Barral, Y. (2009). Septins and the lateral compartmentalization of eukaryotic membranes. Dev. Cell *16*, 493–506.

Chandler, D.E., Hsin, J., Harrison, C.B., Gumbart, J., and Schulten, K. (2008). Intrinsic curvature properties of photosynthetic proteins in chromatophores. Biophys. J. *95*, 2822–2836.

Cobbold, C., Monaco, A.P., Sivaprasadarao, A., and Ponnambalam, S. (2003). Aberrant trafficking of transmembrane proteins in human disease. Trends Cell Biol. *13*, 639–647.

Daniels, D.R., and Turner, M.S. (2007). Diffusion on membrane tubes: a highly discriminatory test of the Saffman-Delbruck theory. Langmuir *23*, 6667–6670.

Derganc, J. (2007). Curvature-driven lateral segregation of membrane constituents in Golgi cisternae. Phys. Biol. *4*, 317–324.

Domanov, Y.A., Aimon, S., Toombes, G.E., Renner, M., Quemeneur, F., Triller, A., Turner, M.S., and Bassereau, P. (2011). Mobility in geometrically confined membranes. Proc. Natl. Acad. Sci. USA *108*, 12605–12610.

Fosnaric, M., Iglic, A., and May, S. (2006). Influence of rigid inclusions on the bending elasticity of a lipid membrane. Phys. Rev. E Stat. Nonlin. Soft Matter Phys. *74*, 051503.

Gonen, T., Cheng, Y., Sliz, P., Hiroaki, Y., Fujiyoshi, Y., Harrison, S.C., and Walz, T. (2005). Lipid-protein interactions in double-layered two-dimensional AQP0 crystals. Nature *438*, 633–638.

Hägerstrand, H., Mrówczyńska, L., Salzer, U., Prohaska, R., Michelsen, K.A., Kralj-Iglic, V., and Iglič, A. (2006). Curvature-dependent lateral distribution of raft markers in the human erythrocyte membrane. Mol. Membr. Biol. *23*, 277–288.

Heinrich, M., Tian, A., Esposito, C., and Baumgart, T. (2010). Dynamic sorting of lipids and proteins in membrane tubes with a moving phase boundary. Proc. Natl. Acad. Sci. USA *107*, 7208–7213.

Hsieh, W.-T., Hsu, C.-J., Capraro, B.R., Wu, T., Chen, C.-M., Yang, S., and Baumgart, T. (2012). Curvature sorting of peripheral proteins on solid-supported wavy membranes. Langmuir *28*, 12838–12843.

Hu, J.J., Shibata, Y., Voss, C., Shemesh, T., Li, Z.L., Coughlin, M., Kozlov, M.M., Rapoport, T.A., and Prinz, W.A. (2008). Membrane proteins of the endoplasmic reticulum induce high-curvature tubules. Science *319*, 1247–1250.

Jiang, Y., Lee, A., Chen, J., Ruta, V., Cadene, M., Chait, B.T., and MacKinnon, R. (2003). X-ray structure of a voltage-dependent K+ channel. Nature *423*, 33–41.

Lai, H.C., and Jan, L.Y. (2006). The distribution and targeting of neuronal voltage-gated ion channels. Nat. Rev. Neurosci. *7*, 548–562.

Leibler, S. (1986). Curvature instability in membranes. J. Phys. *47*, 507–516.

Markin, V.S. (1981). Lateral organization of membranes and cell shapes. Biophys. J. *36*, 1–19.

McMahon, H.T., and Gallop, J.L. (2005). Membrane curvature and mechanisms of dynamic cell membrane remodelling. Nature *438*, 590–596.

Nägerl, U.V., Willig, K.I., Hein, B., Hell, S.W., and Bonhoeffer, T. (2008). Live-cell imaging of dendritic spines by STED microscopy. Proc. Natl. Acad. Sci. USA *105*, 18982–18987.

Netz, R.R., and Pincus, P. (1995). Inhomogeneous fluid membranes: segregation, ordering, and effective rigidity. Phys. Rev. E Stat. Phys. Plasmas Fluids Relat. Interdiscip. Topics *52*, 4114–4128.

Parthasarathy, R., Yu, C.H., and Groves, J.T. (2006). Curvature-modulated phase separation in lipid bilayer membranes. Langmuir *22*, 5095–5099.

Ramadurai, S., Holt, A., Krasnikov, V., van den Bogaart, G., Killian, J.A., and Poolman, B. (2009). Lateral diffusion of membrane proteins. J. Am. Chem. Soc. *131*, 12650–12656.

Reeves, D., Ursell, T., Sens, P., Kondev, J., and Phillips, R. (2008). Membrane mechanics as a probe of ion-channel gating mechanisms. Phys. Rev. E Stat. Nonlin. Soft Matter Phys. *78*, 041901.

Singh, P., Mahata, P., Baumgart, T., and Das, S.L. (2012). Curvature sorting of proteins on a cylindrical lipid membrane tether connected to a reservoir. Phys. Rev. E Stat. Nonlin. Soft Matter Phys. *85*, 051906.

Sorre, B., Callan-Jones, A., Manneville, J.-B., Nassoy, P., Joanny, J.F., Prost, J., Goud, B., and Bassereau, P. (2009). Curvature-driven lipid sorting needs proximity to a demixing point and is aided by proteins. Proc. Natl. Acad. Sci. USA *106*, 5622–5626.

Sorre, B., Callan-Jones, A., Manzi, J., Goud, B., Prost, J., Bassereau, P., and Roux, A. (2012). Nature of curvature coupling of amphiphysin with membranes depends on its bound density. Proc. Natl. Acad. Sci. USA *109*, 173–178.

Tian, A., and Baumgart, T. (2009). Sorting of lipids and proteins in membrane curvature gradients. Biophys. J. *96*, 2676–2688.

van Meer, G., and Sprong, H. (2004). Membrane lipids and vesicular traffic. Curr. Opin. Cell Biol. *16*, 373–378.

van Meer, G., Voelker, D.R., and Feigenson, G.W. (2008). Membrane lipids: where they are and how they behave. Nat. Rev. Mol. Cell Biol. *9*, 112–124.

Veatch, S.L., Cicuta, P., Sengupta, P., Honerkamp-Smith, A., Holowka, D., and Baird, B. (2008). Critical fluctuations in plasma membrane vesicles. ACS Chem. Biol. *3*, 287–293.

Zampighi, G.A., Eskandari, S., Hall, J.E., Zampighi, L., and Kreman, M. (2002). Micro-domains of AQP0 in lens equatorial fibers. Exp. Eye Res. *75*, 505–519.